AUT Journal of Mechanical Engineering

AUT J. Mech. Eng., 8(4) (2024) 337-350
DOI: 10.22060/ajme.2024.23314.6122

Optimization of multilayer perceptron neural network structure for simulating the effect of input variables on the spring-back phenomenon in the ultrasonic vibration assisted single point incremental forming

Mahdi Vahdati *, Seyyed Mojtaba Varedi-Koulaei

Faculty of Mechanical Engineering, Shahrood University of Technology, Shahrood, Iran

ABSTRACT: Applying the ultrasonic vibration to the forming tool in single point incremental forming reduces the forming force, increases the sheet formability, and reduces the spring-back. In the present research, with the aim of minimizing the sheet spring-back, the optimal structure of the multilayer perceptron neural network was extracted using three algorithms which are genetic algorithm, imperialistic competition algorithm, and equilibrium optimizer. Analyzing the optimal network with an R-value of 0.99973 and a root mean squared error of 0.0084 shows that the optimized network performs excellently in simulating the considered system. Then, the best network was used to optimize the variables affecting the objective functions. These objective functions include the average of measured depth (H_{ave}) and the spring-back coefficient (K). The input variables are: vertical step size, sheet thickness, tool diameter, wall inclination angle, and tool feed rate. The results showed that the optimized multilayer perceptron network can simulate the process with very good precision. Also, the extraction of optimal values shows that the maximum of H_{ave} and the minimum of K can be achieved with very good accuracy. Finally, the comparison of the three algorithms showed that the performance of the equilibrium optimizer was better in optimizing the neural network structure. On the other hand, in the optimizing process of the input variables, the imperialistic competition algorithm has been more efficient.

Review History:

Received: Jul. 01, 2024
Revised: Sep. 16, 2024
Accepted: Nov. 08, 2024
Available Online: Nov. 23, 2024

Keywords:

Incremental Forming
Ultrasonic Vibration
Spring-Back Phenomenon
Artificial Intelligence
Evolutionary Algorithms

1- Introduction

Incremental forming has been introduced as one of the rapid prototyping methods [1]. In this process, the specimen geometry is divided into a set of 2D layers, and a local and continuous plastic deformation is applied to the sheet by a hemispherical-head tool. After finishing the forming of each layer, the tool is moved by a small step and repeats the process for the next layer [2]. In the SPIF process, the sheet is simply clamped in the fixture and can be freely bent during the process. Therefore, when the tool force is removed, the effect of spring-back will appear [3]. Hence, spring-back is one of the most significant factors affecting the accuracy of products, and necessary measures should be taken to control and reduce it.

Deokar et al. [4] studied the behavior of force and spring-back in incremental forming using FEA. The results showed that in order to reduce the spring-back, the clamping of the part should be close to the border of the tool path. Ashokkumar et al. [5] studied the effect of spindle speed, tool feed rate, tool diameter, and step size in the incremental forming of conical geometry. They considered thinning rate, surface roughness, spring-back, and sheet formability as the response parameters. The results of the Taguchi and TOPSIS method showed that the spindle speed of 2000 rpm, the feed rate of 300 mm/min, the tool diameter of 10 mm, and the step size of 0.4 mm reduce the surface roughness and spring-back. In a review paper, Patel and Gandhi [6] investigated the effect of incremental forming parameters on the forming forces, formability, spring-back, and surface roughness. They provided a comprehensive assessment of the current state of this process along with technical advantages and existing limitations. On the other hand, the positive effects of ultrasonic vibration include reducing the yield strength of the material [7], reducing the forming force [8], reducing the spring-back [9], reducing the surface roughness [10] and increasing the material formability [11] has been confirmed in the various forming processes. Hence, Vahdati et al. [12] developed the ultrasonic vibration-assisted SPIF (UVaSPIF). The results showed that the applying of ultrasonic vibration to the hemispherical-head tool decreases the forming force, spring-back, and surface roughness. In this direction and in order to understand the effect of ultrasonic vibration in incremental forming, extensive investigation was done by the researchers [13-15]. In another study, Vahdati et al. [16] statistically and

*Corresponding author's email: vahdati@shahroodut.ac.ir

Table 1. Introduction of UVaSPIF input variables [16]

Variable	Symbol	Unit	-1	0	+1
Vertical step size	v	mm	0.25	0.5	0.75
Sheet thickness	t	mm	0.4	0.7	1
Tool diameter	d	mm	10	15	20
Wall inclination angle	φ	degree	40	50	60
Feed rate	f	mm/min	1500	2000	2500

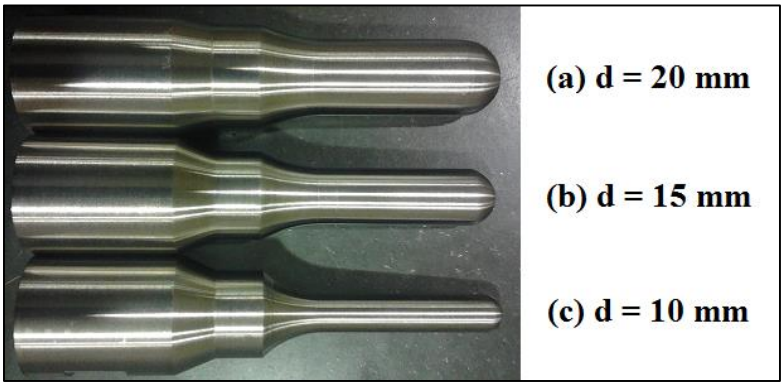

Fig. 1.Hemispherical-head tools

experimentally studied the parameters affecting the spring-back in the UVaSPIF. For this purpose, the factors: vertical step size, sheet thickness, tool diameter, wall inclination angle, and tool feed rate were selected as the input factors. A number of 46 tests were designed and implemented using the response surface methodology (RSM). Then, the average of measured depth (H_{ave}) and the spring-back coefficient (K) of the specimens were considered as the response parameters. The results showed that the fitted models and the regression equations have the essential ability and accuracy to describe and predict the changes of the response parameters.

On the other hand, the ability of evolutionary algorithms based on AI to optimize the objective functions in engineering problems has been confirmed [17-19]. In addition, the optimization of the neural network structure in order to reduce network error and improve its performance has been considered [19-21]. Therefore, in this research, using the reported values of H_{ave} and K in reference [16], the best structure of the MLP neural network is extracted to simulate the existing data. Then, this improved network is used to optimize the variables affecting the spring-back phenomenon. It should be noted that the optimization processes will be performed using GA, ICA, and EO algorithms and their efficiency will be evaluated and compared.

2- Design and implementation of experimental tests

Table 1 shows the input variables of the experimental tests. Each of these variables was considered at three levels.

The vibration amplitude and rotational speed of the tools were set at 7.5 microns and 125 rpm, respectively. To apply the ultrasonic vibration, a generator with a power of 1000 watts and a frequency of 20 kHz was used. Hemispherical-head tools were fabricated in diameters of 10, 15, and 20 mm (Fig. 1).

The experimental tests were designed based on the RSM [22] and using the Minitab software [23]. Details of the design of experiments (DOE) are available in reference [16]. The specimens are made of Al 1050-O, which will be formed as an incomplete pyramid with a depth of 30 mm (Figs. 2 and 3). Experimental tests were performed according to the 46 runs and specimens were produced according to the desired geometry and strategy (Fig. 4).

To evaluate the spring-back, a parameter called spring-back coefficient (K) is used, which is obtained from the following equation [24]:

$$K = \frac{H + \frac{t}{2}}{H_{ave} + \frac{t}{2}} \quad (1)$$

In this equation, H is the applied depth by the forming tool (30 mm), t is the sheet thickness, and H_{ave} is the average of measured depth after removing the tool pressure (Fig. 5). Therefore, as the value of the K parameter approaches to one, the spring-back reduces.

The depth of specimens was measured using the contour-

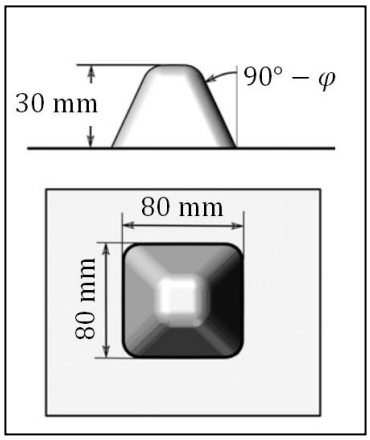

Fig. 2. Dimensional characteristics of the specimen [16]

Fig. 3. Execution of the UVaSPIF process [16]

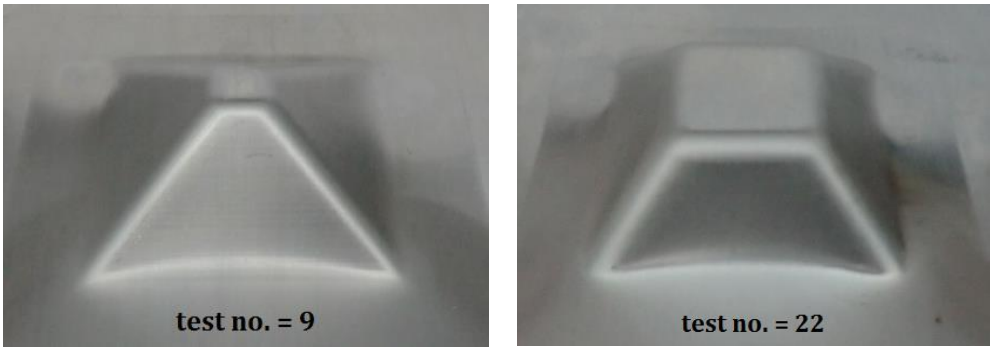

(a) Test no. = 9 (b) Test no. = 22

Fig. 4. Two formed specimens [16]

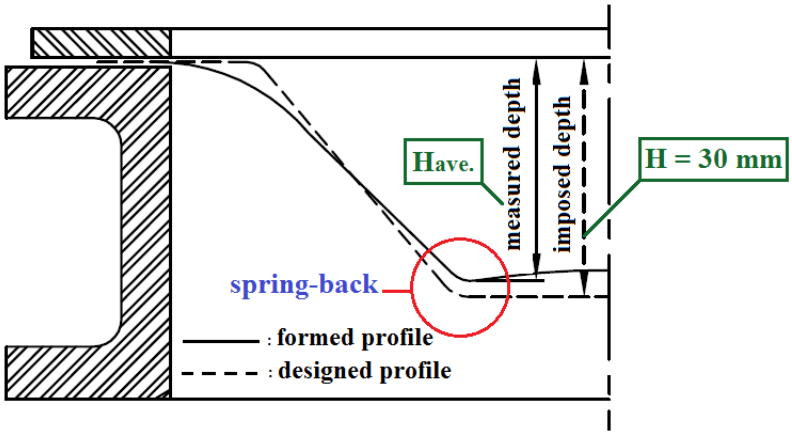

Fig. 5. The imposed depth (H) and the measured depth (H_{ave})

Table 2. Used optimization algorithms in this research

No.	Algorithm	Category	Proposed Year	Main Ref.
1	GA	Evolution-based algorithm	1970	[26]
2	ICA	human-based algorithm	2007	[27]
3	EO	physics-based algorithm	2020	[28]

graph device, and its average was registered as the H_{ave}. Then, using Eq. 1, the spring-back coefficient (K) was calculated and the values of the response parameters were recorded [16].

3- Optimizing the structure of the neural network

3- 1- Optimization Algorithms

Metaheuristic techniques are methods that use real-life events to make a computer program that helps find the best solutions for problems. These methods are grouped into four main categories: methods based on evolution, methods based on physics, methods based on swarms, and methods based on humans [25]. In evolution-based algorithms, the guidelines of natural evolution are followed, while in physics-based algorithms, the laws of nature are replicated. The swarm-based methods include algorithms that imitate how animals work together in a group. Finally, human-based algorithms, are influenced by how people behave socially.

In this research, the optimization problem is addressed through the employment of three distinct methodologies: the genetic algorithm (GA), the imperialistic competition algorithm (ICA), and the equilibrium optimizer (EO) technique. Should note that these algorithms fall into different categories, as shown in Table 2. An overview of these optimization algorithms is in Refs. [26-28].

3- 2- Network's structure

For simulating the system defined in the previous section using machine learning algorithms, a multi-layer perceptron (MLP) network based on the different hidden layers is utilized. The considered training algorithm is the back Propagation (BP) algorithm [29]. The neurons' number in the input and output layers of the network are defined regarding the number of inputs and outputs of the system. But hidden layers' characteristics can be chosen arbitrarily: their number, their neurons' number, and their transfer functions type. Thus, one can optimize the network's structure to generate an optimal network and get the best performance.

In the present research, an optimization problem is defined for designing the MLP network with an optimal structure. This problem is established based on the following basis:

- The problem's design variables include the number of neurons and the type of transfer function for each hidden layer.
- The margin of variation for neurons' number is selected between 1 to 30.
- The transfer functions are limited to three types: *logsig*, *tansig*, and *elliotsig*.
- The cost function is defined based on the Root Mean Squared Error (*RMSE*) of the network.
- The optimization process is performed for networks with two, three, four, and five hidden layers networks.

There is no need to make any improvements or adjustments for the network consisting of just one hidden layer; its possible cases are equal to 90, and one can select the optimal solution by checking all cases. Except for the network with one hidden layer, the optimization problem for other networks has 2**HL* design variables, if *HL* is defined as the number of hidden layers.

Three choices are available for the selection of the transfer function, based on Table 3. Moreover, the neural network's error, defined as *RMSE*, has the following equation:

$$RMSE = \sqrt{\frac{1}{n}\sum\left(Y_d - Y_p\right)^2} \tag{2}$$

In this equation, n is the number of samples, while Y_p and Y_d are the predicted and desired outputs, respectively. Also, there is another criterion (R) that shows the performance of the network, which is defined as follows:

$$R = \sqrt{1 - \frac{\sum\left(Y_d - Y_p\right)^2}{\sum\left(Y_d - \overline{Y_d}\right)^2}} \tag{3}$$

Where $\overline{Y_d}$ is the mean value of Y_d. Should note that the minimum value of *RMSE* (*RMSE*=0) is equivalent to the maximum value of R (R=1).

Based on the above explanations, now the summary of the defined optimization problem can be represented as follows:

Table 3. Different transfer function types considered for the optimization process

Name of transfer function	Equation
Log-sigmoid (*Logsig)*	$F_{logsig}(x)=\frac{1}{1+e^{-x}}$
Hyperbolic tangent sigmoid (*Tansig)*	$F_{\tan sig}(x)=tanh(x)=\frac{e^{x}-e^{(-x)}}{e^{x}+e^{(-x)}}$
Elliot symmetric sigmoid (*Elliotsig)*	$F_{elliotsig}(x)=\frac{x}{1+\lvert x\rvert}$

$$
\begin{aligned}
&Min \quad RMSE\left(X_j\right),\\
&X_j:\left\{N_i,F_i\right\}\\
&S.t: \quad 1<N_i<30\\
&\qquad F_i\in\left\{logsig,tansig,elliotsig\right\}\\
&*\ \ HL=2:\ j=2,\quad i=1,2\\
&*\ \ HL=3:\ j=3,\quad i=1,2,3\\
&*\ \ HL=4:\ j=4,\quad i=1,\ldots,4\\
&*\ \ HL=5:\ j=5,\quad i=1,\ldots,5
\end{aligned}
\tag{4}
$$

Where N_i indicates the number of neurons in the ith hidden layer, and F_i shows the type of transfer function for the ith hidden layer's neurons. In addition, X_j is the vector of design variables to optimize the network whose number of hidden layers is equal to j.

Based on the information gathered, it was determined that there are a total of 46 samples, and this system has five inputs (v, t, d, φ, f) and two outputs (H_{ave}, K). For entering the data into the neural network's training process, the extracted experimental data is divided into three parts, in a random way: 70% is allocated for the training set, 15% is selected for the validation set, and the remaining 15% are used for the test set. Moreover, all data is normalized between 0 to 1, and the network was trained using the Levenberg-Marquardt (LM) approach.

Before optimizing the MLP network by adding more hidden layers (2, 3, 4, and 5), the results for the network with only one hidden layer are described. When HL=1, N_1 and F_1 are two design parameters of the problem. Given that the design parameters are discrete variables, and knowing N_1 and F_1 have 30 and 3 discrete levels, respectively, there are only 90 different vectors in the design space of this problem. Thus, one can test all the design vectors, and select the optimal one with the lowest level of *RMSE*, without any optimization process. The findings indicate that the optimal network has N_1=8 neurons in its hidden layer, and *elliotsig* is its transfer function. Based on this structure, the values of *RMSE* and are equal to 0.0221 and 0.99798, respectively.

4- Results

4- 1- Network optimization

In this section, we studied and improved the MLP neural network. We tried different numbers of hidden layers: two, three, four, and five. We used optimization algorithms to make the network more accurate by reducing its *RMSE*. For the optimization process, the population size is considered twice the number of design variables, while the maximum number of iterations for all metaheuristic algorithms is equal to 100.

The plots of Fig. 6 represent the convergence curve of the three metaheuristic algorithms, for optimizing the MLP network with different numbers of hidden layers. These figures signify that in the networks with 2, 3, and 4 hidden layers, the EO algorithm attains superior outcomes compared to others, while for the network with 5 hidden layers, the ICA algorithm demonstrates a more favorable performance.

Table 4 shows the detailed results, including the optimal structures of networks, in addition to their *RMSE* and *R*'s value for all cases. Moreover, these results are compared with the best solution for the network with one hidden layer. Furthermore, Fig. 7 compares the *RMSE* and *R* values of various algorithms with different hidden layer networks.

Considering the reported results, the three hidden layers network shows superior performance compared to the other types, while the EO was the best among the optimization techniques. Also, one can see that the network with three hidden layers, found using the EO algorithm, is the best among all the different networks. This optimal network, with three hidden layers, has a 61.99% error reduction compared to the one-hidden-layer network.

• The summarized optimization outcomes considering

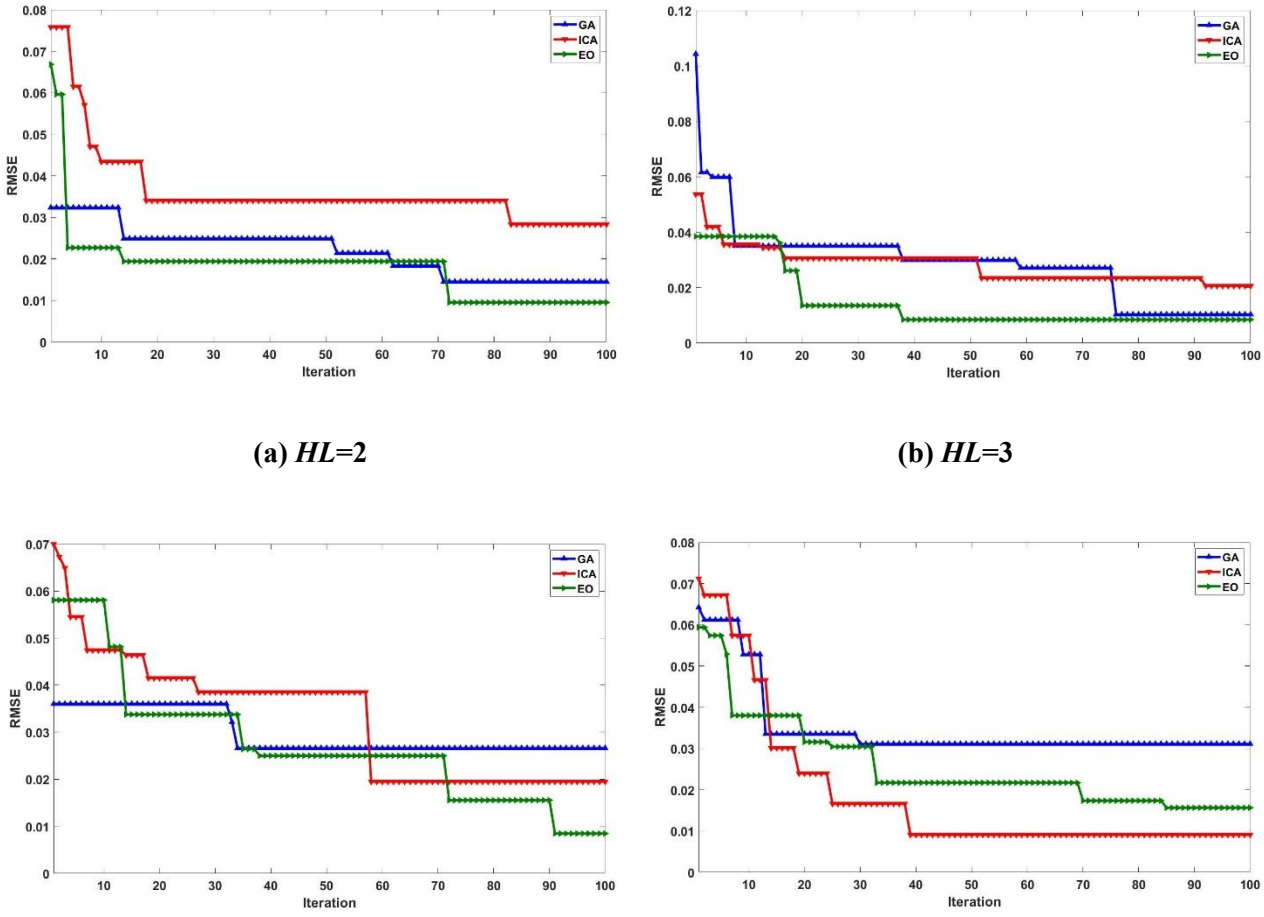

(a) *HL*=2 **(b) *HL*=3**

(c) *HL*=4 **(d) *HL*=5**

Fig. 6. Performance evolution for different networks

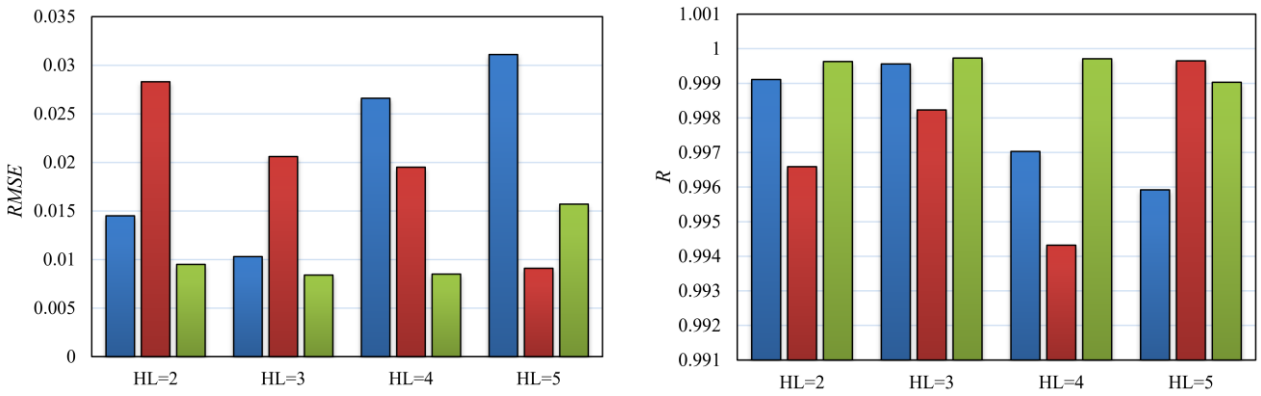

(a) *RMSE* **(b) *R***

Fig. 7. Comparison of the obtained results (GA ICA EO)

Table 4. Detailed results of optimizing MLP networks in different cases

Network	Algorithms	N_i	F_i	*RMSE*	*R*
HL=1	---	8	elliotsig	0.0221	0.99798
HL=2	GA	[8 1]	[tansig logsig]	0.0145	0.99911
	ICA	[30 4]	[tansig logsig]	0.0283	0.99659
	EO	[6; 6]	[logsig; tansig]	0.0095	0.99963
HL=3	GA	[3; 12; 9]	[tansig; tansig; logsig]	0.0103	0.99956
	ICA	[10; 25; 4]	[logsig; logsig; elliotsig]	0.0206	0.99823
	EO	[5; 2; 2]	[tansig; elliotsig; elliotsig]	0.0084	0.99973
HL=4	GA	[5; 10; 8; 19]	[tansig; tansig; logsig; elliotsig]	0.0266	0.99703
	ICA	[15; 12; 20; 4]	[tansig; tansig; logsig; tansig]	0.0195	0.99432
	EO	[3; 6; 13; 7]	[tansig; tansig; logsig; logsig]	0.0085	0.99971
HL=5	GA	[11; 24; 14; 6; 16]	[logsig; logsig; logsig; logsig; tansig]	0.0311	0.99592
	ICA	[2; 10; 13; 26; 18]	[tansig; logsig; tansig; tansig; logsig]	0.0091	0.99965
	EO	[5; 1; 3; 1; 1]	[tansig; logsig; elliotsig; tansig; tansig]	0.0157	0.99903

different network types and different optimization methods are:

- The EO algorithm is the most accurate method for networks with 2, 3, and 4 hidden layers, while the ICA algorithm is better for five hidden layers.
- Comparing three optimization methods, the EO, a novel algorithm developed in 2020, has the best results.
- Networks that have three hidden layers show superior performance compared to those with fewer or more hidden layers.
- The three hidden layers MLP network, acquired by the EO algorithm, has the smallest amount of *RMSE* compared to all other improved networks (*RMSE*=0.0084).

4- 2- Optimal network error analysis

According to the results, represented in the previous section, the best network designed from the optimization process was a three-hidden layers network acquired by the EO algorithm. The organization of this network can be seen in Fig. 8. It is now possible to evaluate the performance of this network by an error analysis.

Fig. 9 shows the location of the optimal network's output with respect to the problem's target. Figs. 9(a) and 9(b) show this diagram for the first and second outputs, H_{ave} and K, while in Fig. 9(c), the regression diagram is plotted for both outputs in the normalized format. The *R's* value greater than 0.999 shows that the optimized network has excellent performance for simulating the considered system.

Moreover, Figs. 10 and 11 represent the absolute error and the error histogram for two different outputs. Based on Fig. 10, the maximum absolute error for two errors, H_{ave} and K, are equal to 11×10^{-4} and 4×10^{-4}, respectively.

According to these findings, it can be concluded that the obtained network can simulate the desired problem with minimal error. Also, the two outputs' errors are at the same level, which means that there is not a large difference between the outputs' accuracy.

5- Design process: optimizing input parameters for a targeted output

This section aims to extract some optimal values for input parameters of the system, based on the desired values for their outputs. This design process can be converted to an optimization problem, in which its objective function is maximizing the first output (H_{ave}) and minimizing the second one (K). Because these two outputs are dependent on each other, one can sum these objective functions.

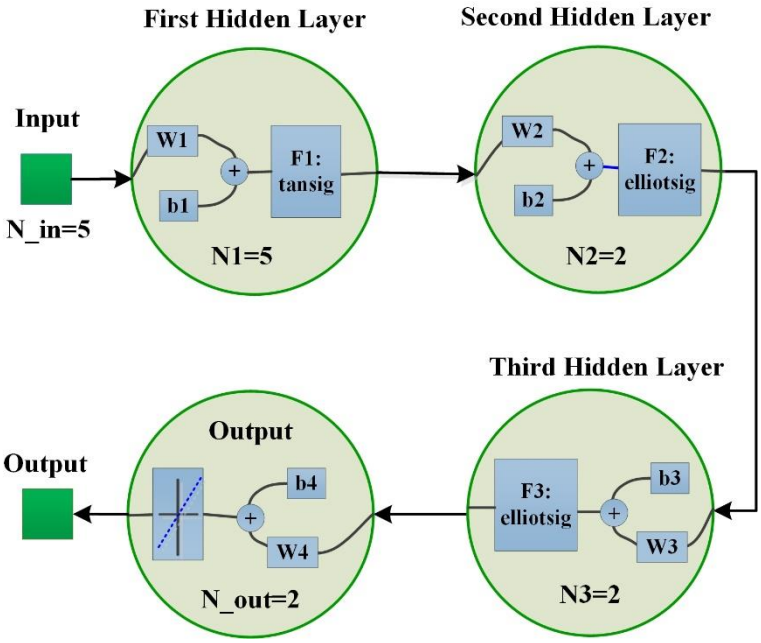

Fig. 8. The optimal structure of the MLP network

This new optimization problem is totally different from the optimization problem of the previous section but uses its optimal network. In the other word, for calculating the system's outputs in this section, the optimal MLP network gained in the previous section is utilized. Here, the design parameters are the five inputs of the considered system, including *v, t, d, φ,* and *f*. Therefore, the second optimization problem of this research, defined as a process design, is as follows:

$$\begin{aligned} &\text{Min } F_{obj}(X) = \frac{1}{f_1} + f_2 \\ &X : \{\text{v, t, d, } \varphi\text{, f}\} \\ &\text{S.t} : Lb < x_i < Ub \quad i = 1 \ldots 5 \end{aligned} \tag{5}$$

Where $f_1 = H_{ave}$ and $f_2 = K$, and *Lb* and *Ub* are the lowest and highest values taken from the data samples. For minimizing the defined objective function in this section, all three algorithms, including GA, ICA, and EO, are utilized. This optimization problem has been solved several times by means of each optimization algorithm, and the five best results for each one are represented in Table 5. These results show that the values of H_{ave} and *K* in different methods and different runs are near to each other and there is not a sensible difference between them, while their optimal input variables are different. Thus, this optimization problem has many solutions. In Fig. 12, the optimized inputs are shown based on the 15 different runs. Note that this figure has been plotted in the format of the normalized data.

6- Conclusion

In this research, the structure of the MLP neural network was extracted and optimized in order to predict the spring-back in the UVaSPIF. Neural network training was done based on the reported data in reference [16]. Next, the neural network was used to optimize the input variables and to maximize the average of measured depth (H_{ave}), and minimize the spring-back coefficient (*K*). Optimization processes were performed using three powerful and well-known algorithms, namely GA, ICA, and EO. The findings of this study are summarized in the following way:

- The values of *RMSE*=0.0084 and *R*=0.9997 obtained from the optimized neural network showed that this network has succeeded in predicting the response parameters with high accuracy.
- In the optimization process of the neural network structure, the EO algorithm has better performance.
- The optimization results of the neural network structure showed that the network error increases with the increase in the number of hidden layers. Therefore, the best results were obtained with the number of 3 and 4 hidden layers.

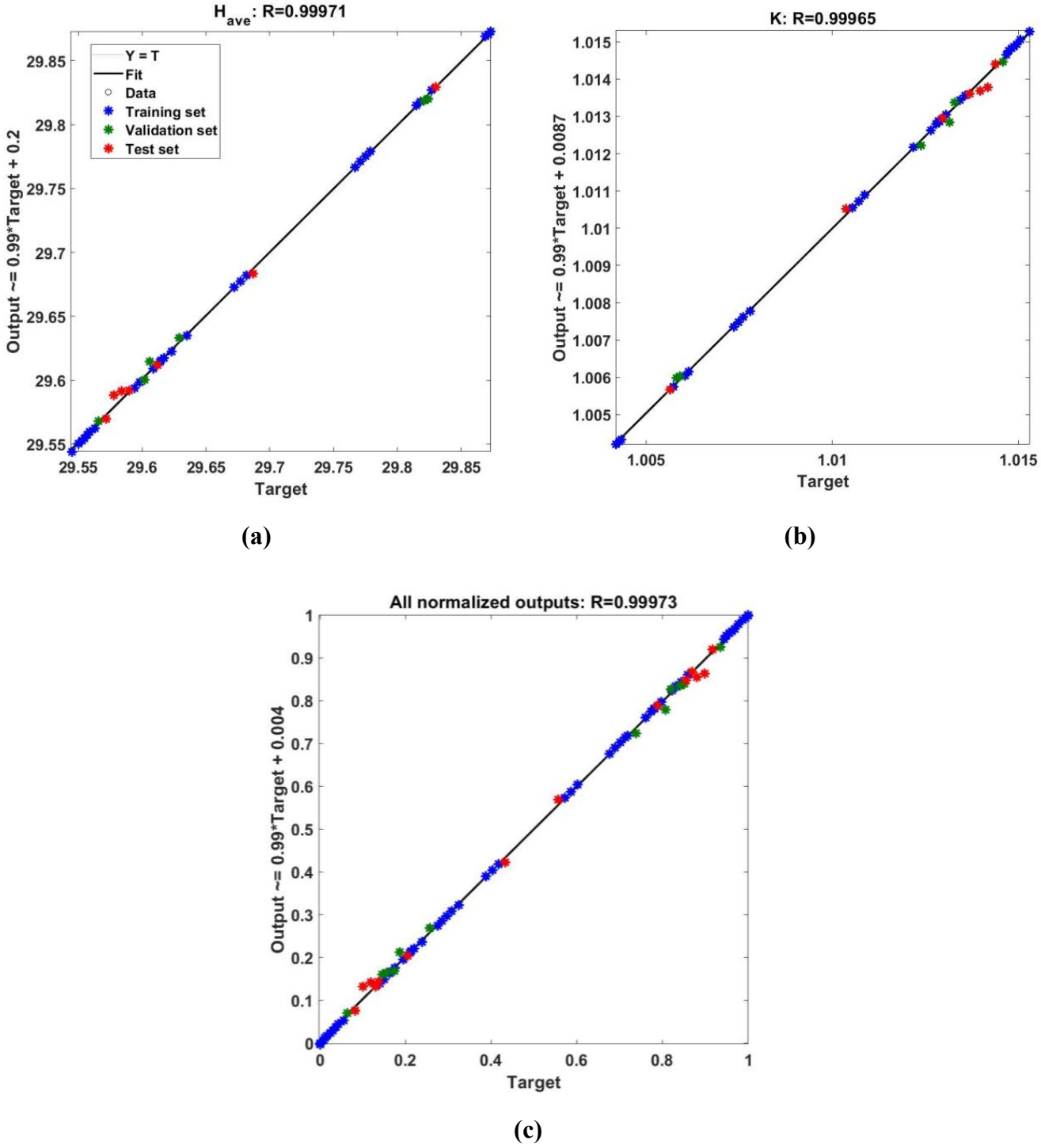

Fig. 9. The location of the predicted output against its target for the best network. (a) First output, H_{ave}, (b) Second output, K, (c) Both outputs, in the normalized format

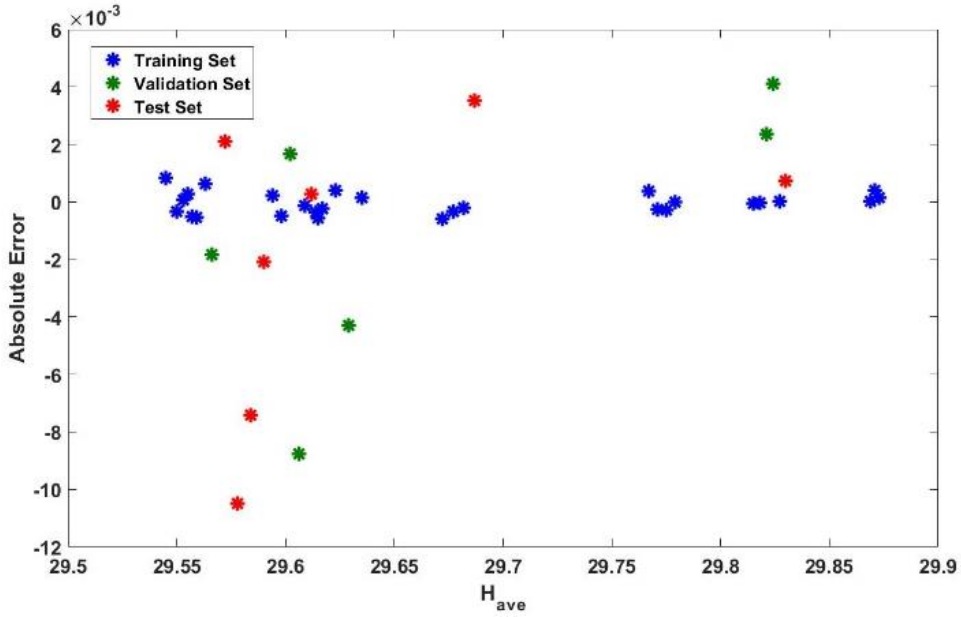

(a)

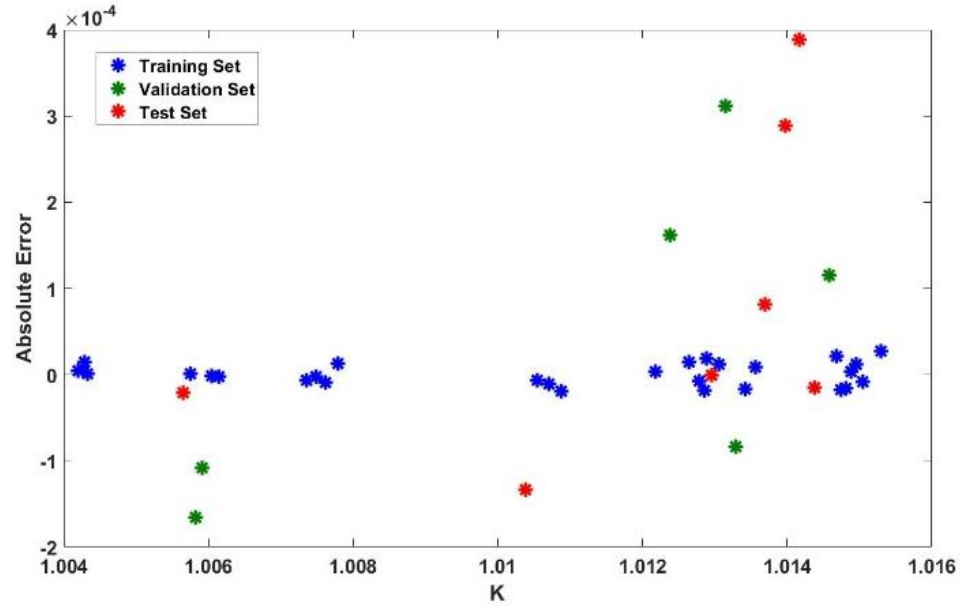

(b)

Fig. 10. The absolute error of the predicted outputs using best network. (a) First output, H_{ave} (b) Second output, K

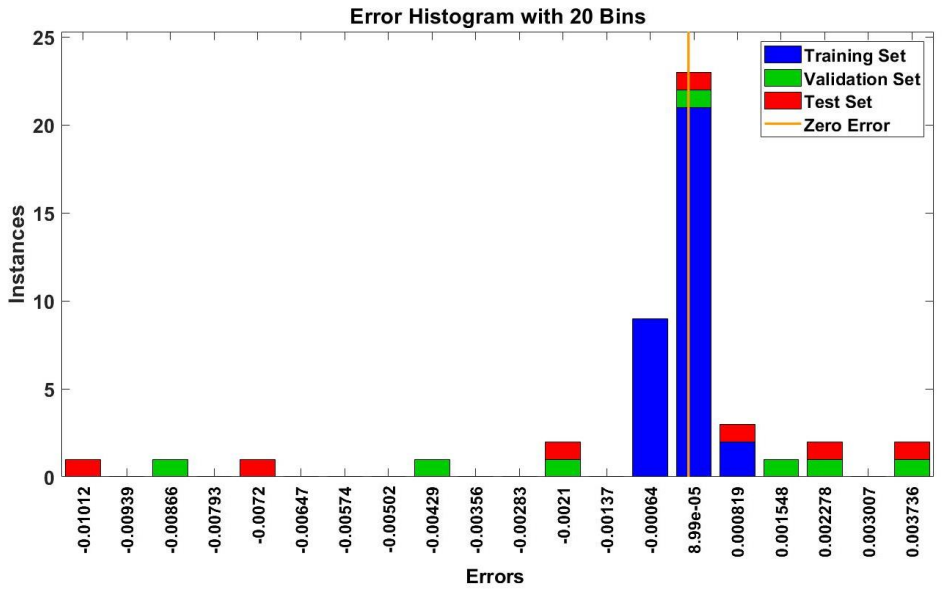

(a)

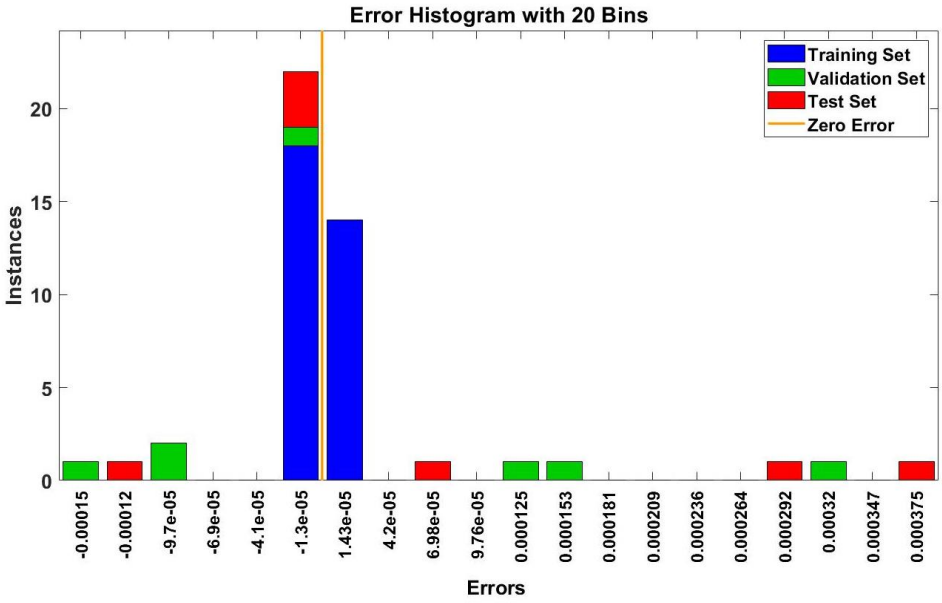

(b)

Fig. 11. The error histogram of the predicted outputs using the best network. (a) First output, H_{ave}, (b) Second output, K

Table 5. Optimization results of the design process

Algorithm	v	t	d	φ	f	$f_1 = H_{ave}$	$f_2 = K$
GA	0.25	0.610365	10.42029	45.96913	1846.395	29.87284	1.00E+00
	2.66E-01	0.580647	10	40.2103	2083.953	29.87283	1.00E+00
	0.436514	0.894978	10	53.46541	1753.091	29.87282	1.00E+00
	0.250026	0.910462	12.66883	52.65976	1927.858	29.87282	1.00E+00
	0.465487	0.893506	10.05626	53.67196	1558.011	29.87281	1.0042
ICA	0.315779	0.683831	10.13686	51.02141	1728.328	29.87284	1.00E+00
	0.284198	0.714057	10.48811	41.12143	2311.118	29.87283	1.00E+00
	0.288474	0.702546	10	47.55525	2038.146	29.87283	1.00E+00
	0.25	0.70303	10	40	2500	29.87283	1.00E+00
	0.250857	0.72024	10	40.84809	2500	29.87283	1.00E+00
EO	0.250449	0.53103	10.07309	47.67064	1500	29.87284	1.00E+00
	0.487087	0.997683	1.11E+01	47.52018	1500	29.87282	1.00E+00
	0.503708	1	10	44.38489	1938.6	29.87281	1.0042
	0.25	0.655042	10.79317	54.22639	1501.049	29.87282	1.004201
	0.50461	0.999966	10.15266	40	2189.621	29.87281	1.0042

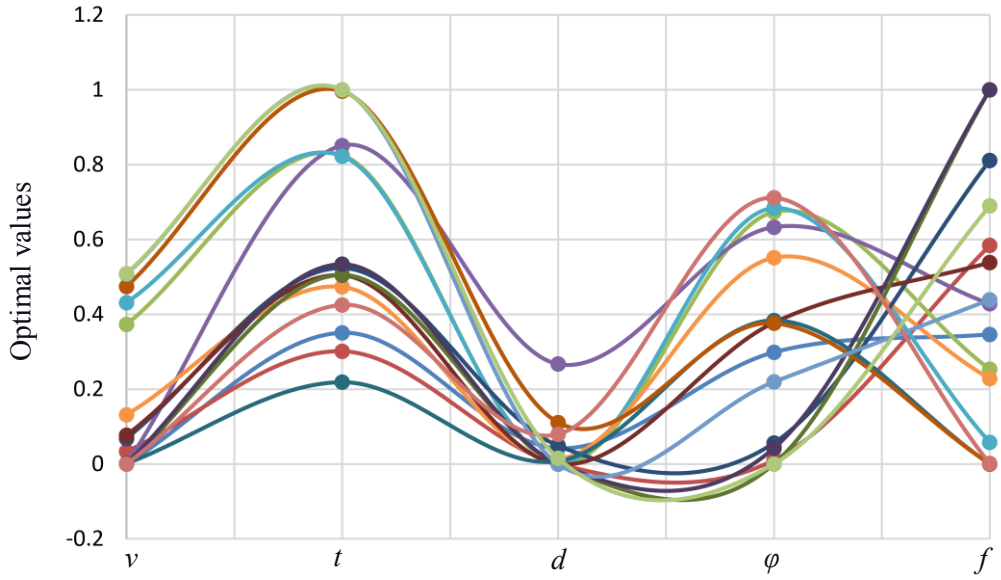

Fig. 12. Optimal values of the input variables in different 15 runs

- During the optimization process, the parameters of H_{ave} and K have been maximized and minimized, respectively, with high precision.
- In the optimizing process of the input variables, the efficiency of the ICA algorithm has been better.

Statements and Declarations

Funding

The authors declare that no funds, grants, or other support were received during the preparation of this manuscript.

Competing Interests

The authors have no relevant financial or non-financial interests to disclose.

Author Contributions

All authors contributed to the study's conception and design. The first draft of the manuscript was written by all authors and they commented on previous versions of the manuscript. All authors read and approved the final manuscript.

References

[1] Z. Chang, M. Yang, J. Chen, Geometric deviation during incremental sheet forming process: Analytical modeling and experiment, International Journal of Machine Tools and Manufacture, 198 (2024) 104160.

[2] R.S. Bhasker, Y. Kumar, Process capabilities and future scope of Incremental Sheet Forming (ISF), Materials Today: Proceedings, 72(3) (2023) 1014-1019.

[3] A. Qadeer, G. Hussain, M. Alkahtani, J. Buhl, Springback behavior of a metal/polymer laminate in incremental sheet forming: stress/strain relaxation perspective, Journal of Materials Research and Technology, 23 (2023) 1725-1737.

[4] S.U. Deokar, P.K. Jain, P. Tandon, A. Pathak, Analysis of Spring back and Force behavior in Single Point Incremental Sheet Forming though FEA, Materials Today: Proceedings, 18 (2019) 3330-3339.

[5] S. Ashokkumar, S.P.S.S. Sivam, S. Balasubramanian, R.V. Nanditta, Effects of process variables optimization on the quality of parts processed in high-speed single point incremental sheet metal forming by ranking algorithm, Materials Today: Proceedings, 45(2) (2021) 1707-1712.

[6] D. Patel, A. Gandhi, A review article on process parameters affecting Incremental Sheet Forming (ISF), Materials Today: Proceedings, 63 (2022) 368-375.

[7] F. Blaha, B. Langenecker, Tensile deformation of zinc crystal under ultrasonic vibration, Naturwiss, 42(20) (1955) 556-556.

[8] T. Jimma, Y. Kasuga, N. Iwaki, O. Miyazawa, E. Mori, K. Ito, H. Hatano, An application of ultrasonic vibration to the deep drawing process, Journal of Materials Processing Technology, 80-81 (1998) 406-412.

[9] J. Tsujino, T. Ueoka, K. Takiguchi, H.S.H. Satoh, K.T.K. Takahashi, Characteristics of bending parts of metal plates using ultrasonic bending systems with a vibration punch and a vibration die, Japanese Journal of Applied Physics, 32 (1993) 2447-2451.

[10] K. Siegert, A. Mock, Wire drawing ultrasonically oscillating dies, Journal of Materials Processing Technology, 60 (1996) 657-660.

[11] M. Susan, L.Gh. Bujoreanu, D.G. Galusca, C. Munteanu, M. Mantu, On the drawing in ultrasonic field of metallic wires with high mechanical resistance, Journal of Optoelectronics and Advanced Materials, 7(2) (2005) 637-645.

[12] M. Vahdati, R. Mahdavinejad, S. Amini, Investigation of the ultrasonic vibration effect in incremental sheet metal forming process, Proceedings of the Institution of Mechanical Engineers, Part B: Journal of Engineering Manufacture, 231(6) (2017) 971-982.

[13] Y. Long, Y. Li, J. Sun, I. Ille, J. Li, J. Twiefel, Effects of process parameters on force reduction and temperature variation during ultrasonic assisted incremental sheet forming process, International Journal of Advanced Manufacturing Technology, 97 (2018) 13-24.

[14] M. Vahdati, Finite Element Analysis and Experimental Study of the Ultrasonic Vibration-assisted Single Point Incremental Forming (UVaSPIF) Process, Iranian Journal of Materials Forming, 6(2) (2019) 30-41.

[15] Z. Cheng, Y. Li, J. Li, F. Li, P.A. Meehan, Ultrasonic assisted incremental sheet forming: Constitutive modeling and deformation analysis, Journal of Materials Processing Technology, 299 (2022) 117365.

[16] M. Vahdati, R.A. Mahdavinejad, S. Amini, Statistical analysis and optimization of factors affecting the spring-back phenomenon in UVaSPIF process using response surface methodology, International Journal of Advanced Design and Manufacturing Technology, 8(1) (2015) 13-23.

[17] K. Mori, M. Yamamoto, K. Osakada, Determination of hammering sequence in incremental sheet metal forming using a genetic algorithm, Journal of Materials Processing Technology, 60(1-4) (1996) 463-468.

[18] T. Sathish, GAC-ANN Technique for Prediction of Spring Back Effect in Wipe Bending Process of Sheet Metal, Materials Today: Proceedings, 5 (2018) 14448-14457.

[19] S. Moradi, M. Gerdooei, S.M. Varedi-Koulaei, H.G. Nosrati, MLP neural network with an optimal architecture for modeling the ECAP-C process, Neural Computing and Applications, 35 (2022) 2701-2715.

[20] M. Nazari, S.M. Varedi-Koulaei, M. Nazari, Flow characteristics prediction in a flow-focusing microchannel for a desired droplet size using an inverse model: experimental and numerical study, Microfluidics and Nanofluidics, 26(4) (2022) 1-19.

[21] M. Ghazvini, S.M. Varedi-Koulaei, M.H. Ahmadi, M.

Kim, Optimization of MLP neural network for modeling flow boiling performance of Al2O3/water nanofluids in a horizontal tube, Engineering Analysis with Boundary Elements, 145 (2022) 363-395.

[22] F. Jarahi, M. Vahdati, R. Abedini, Modeling and Optimization of Shear Strength of the Welded Joint Produced by Ultrasonic Welding of Copper Wire to Aluminum Sheet, Transactions of the Indian Institute of Metals, 77 (2024) 2499-2508.

[23] Minitab software, www.minitab.com

[24] M. Vahdati, M. Sedighi, H. Khoshkish, An analytical model to reduce spring back in Incremental Sheet Metal Forming (ISMF) process, Advanced Materials Research, 83-86 (2010) 1113-1120.

[25] M.H. Nadimi-Shahraki, H. Zamani, Z. Asghari Varzaneh, S. Mirjalili, A Systematic Review of the Whale Optimization Algorithm: Theoretical Foundation, Improvements, and Hybridizations, Archives of Computational Methods in Engineering, 30 (2023) 4113–4159.

[26] J.H. Holland, Adaptation in natural and artificial systems: an introductory analysis with applications to biology, control, and artificial intelligence, MIT press, ISBN: 9780262581110, 1992.

[27] E. Atashpaz-Gargari, C. Lucas, Imperialist competitive algorithm: an algorithm for optimization inspired by imperialistic competition, In IEEE congress on evolutionary computation, (2007) 4661-4667.

[28] A. Faramarzi, M. Heidarinejad, B. Stephens, S. Mirjalili, Equilibrium optimizer: A novel optimization algorithm, Knowledge-Based Systems, 191 (2020) 105190.

[29] D.C.E. Saputra, K. Sunat, T. Ratnaningsih, A New Artificial Intelligence Approach Using Extreme Learning Machine as the Potentially Effective Model to Predict and Analyze the Diagnosis of Anemia, Healthcare, 11(5) (2023) 697.

HOW TO CITE THIS ARTICLE

M. Vahdati, S. M. Varedi-Koulaei, Optimization of multilayer perceptron neural network structure for simulating the effect of input variables on the spring-back phenomenon in the ultrasonic vibration assisted single point incremental forming, AUT J. Mech Eng., 8(4) (2024) 337-350.

DOI: 10.22060/ajme.2024.23314.6122